

Biophysical Journal, Volume 99

Supporting Material

How Pancreatic β Cells Discriminate Long- and Short-Time Scale cAMP Signals

Bradford E. Percy and Arthur S. Sherman

S1 Nuclear-Cytoplasmic Ratio

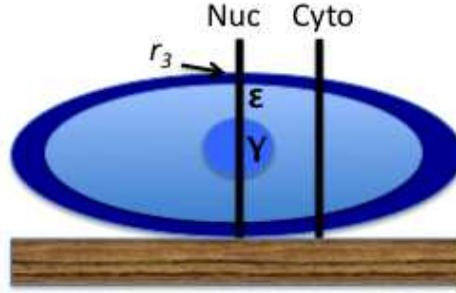


Figure S1: Fluorescent stimulation occurs along the vertical lines. The Nuc measurement then incorporates the region domains: submembrane, cytosol, and nucleus, while the Cyto measurement includes cytosol and submembrane.

S2 Protein Kinase Inhibitor Can Enhance Effect of Reduced Nuclear Membrane Diffusive Flux

We briefly consider an active mechanism of efflux for cPKA in the nucleus via protein Kinase Inhibitor (PKI) such as

$$PKI_{pump} = V_{PKI} C_1 \frac{K_{PKI}^2}{C_1^2 + K_{PKI}^2}$$

where we consider a linear pump with rate V_{PKI} which inhibits at high values of cPKA with sensitivity K_{PKI} . The inhibition is considered in light of the data showing a near even distribution of cPKA after extended exposure to IBMX. This mechanism cannot, by itself, account for the low epi ratio in oscillatory IBMX conditions and high epi ratio in maintained IBMX (data not shown). However, if the sensitivity of the PKI pump is carefully chosen, then the oscillations in pulsatile IBMX are greatly reduced. This is shown in Figure S2 with $V_{PKI} = 1\mu\text{M}/\text{s}$ and $K_{PKI} = 0.0022\mu\text{M}$ (compare with Figure 3(A) in the main text). Pulsatile IBMX results in only a negligible rise in nuclear cPKA when active removal due to PKI is present. In contrast, with a constant IBMX stimulus cPKA overwhelms the PKI-mediated efflux of cPKA and a large build up occurs. If cPKA can be monitored continuously so that oscillations can be observed, it would be possible to test experimentally the model prediction that inhibiting PKI will increase the magnitude of the oscillations in response to pulsatile IBMX. However, the parameter range for this effect is narrow. For $K_{PKI} = 0.003\mu\text{M}$, cPKA cannot overwhelm the PKI-mediated efflux and the Epi ratio never exceeds that of the pulsatile IBMX oscillations, whereas for $K_{PKI} = 0.001\mu\text{M}$ the amplitude of the oscillations is large, as in Fig. 3A in the main text. It should also be noted that even for $K_{PKI} = 0.0022\mu\text{M}$ the system is bistable – the small amplitude oscillations shown in S2 co-exist with those shown in Fig. 3A. Which solution is obtained depends on initial conditions. This generates a form of hysteresis. When the initial conditions are such that $K_{PKI} = 0.0022\mu\text{M}$ yields

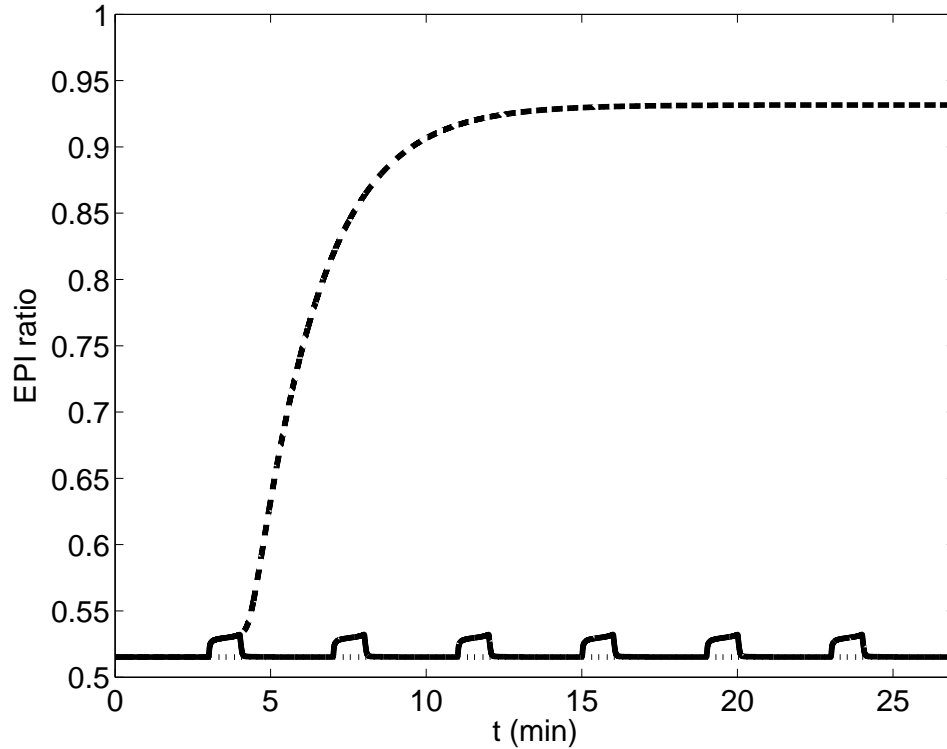


Figure S2: Addition of PKI. Using the initial conditions of the Epi model without PKI we get a rapid equilibration to a lower Epi ratio. The basal state (dotted) is visible beneath the greatly blunted oscillations (solid), while the sustained IBMX stimulus still generates a significant Epi ratio (dashed). Compare with Fig. 3A in the main text.

small amplitude oscillations, changing to $K_{PKI} = 0.001\mu\text{M}$ converts the oscillations to ones like those in Fig. 3A in the main text. Continuing from such large oscillations, if K_{PKI} is changed back to $0.0022\mu\text{M}$ those oscillations persist rather than returning to the small amplitude oscillations. This could also be tested experimentally. If low amplitude (or non-detectable) cPKA oscillations are observed, and a PKI inhibitor increases (or initiates) oscillations, then the oscillations may persist when the inhibitor is removed.

S3 Spatial Model

Model Development

In this section we describe a partial differential equation model for a radially symmetric beta cell that parallels the three-compartment model in the main text. In order to avoid confusion with PDE (phosphodiesterase), we will refer to this as the “spatial model.”

Since cAMP and PDE reactions occur at the membrane, we define a region, equivalent to the submembrane shell in the three-compartment model, within approximately 100nm of the plasma membrane, which corresponds to the

$$\frac{\partial a}{\partial t} = \frac{1}{r^2} \frac{\partial}{\partial r} \left(D_a(r) r^2 \frac{\partial a}{\partial r} \right) - k_{pde_s}(r)a + AC(r) - k_{pde_a}(r)a \quad (\text{S1})$$

in the domain $r \in [0, r_L]$, where r_L is the radius of the cell. There is no flux of cAMP across the cell membrane. The diffusion coefficient is piecewise constant and may be reduced below the cytosolic value at the boundary between the sub-membrane region and the cytosol to create a functional compartment (see Fig. 6 in the main text). Both $AC(r)$ and $k_{pde_a}(r)$ are nonzero only within 100nm of the membrane at $r = r_L$. The soluble PDE is assumed to be active everywhere except in the nucleus (i.e. $k_{pde_s} > 0$ for $r > r_N$ and $k_{pde_s} = 0$ for $r \leq r_N$, where r_N is the radius of the nucleus).

Diffusion of cAMP and PKA

As in the three-compartment model, diffusion of cAMP in the cytosol is unbuffered, but diffusion through the nuclear reduction is reduced for r within the nuclear membrane, and diffusion of rPKA is neglected (see Modeling Methods in main text). For the spatial model, We consider only unlabeled (native) PKA species.

Incorporating the reaction and diffusion of cPKA yields the equations

$$\frac{\partial C}{\partial t} = \frac{1}{r^2} \frac{\partial}{\partial r} \left(D_c(r) r^2 \frac{\partial C}{\partial r} \right) - 2k_a RC^2 + 2k_b(a)(R_T - R) \quad (\text{S2})$$

$$\frac{\partial R}{\partial t} = -k_a RC^2 + k_b(a)(R_T - R), \quad (\text{S3})$$

where R is the concentration of unbound rPKA homodimer, C is the concentration of unbound cPKA monomer, and R_T is the total regulatory subunit concentration. The diffusion coefficient of C , $D_c(r)$, is constant and denoted simply as D_c , except within the nuclear membrane, where it is set to D_N , as in the three-compartment model.

There is no cPKA flux across the plasma membrane. Since we have assumed that rPKA cannot diffuse, R_T at any point in space is constant in time, but the division into free subunits and bound subunits that are incorporated into PKA holoenzymes can vary in space, depending on the local concentration of cAMP. Thus,

$$R_T(r) = R(r, t) + P(r, t),$$

where P is the PKA holoenzyme concentration. We allow the total rPKA to differ in the submembrane boundary and cytosolic compartments:

$$R_T(r) = \begin{cases} R_{bT} & r_b < r < r_L \\ R_{iT} & r_N \leq r \leq r_b \\ 0 & 0 < r < r_N \end{cases}$$

where r_b is the cell radius up to the TIRF zone and is set equal to $r_L - 100\text{nm}$. The regulatory subunits are excluded from the nucleus ($r < r_N$).

Simulations of the Spatial Model

Figure S3 (p. S4) shows the result in time and space of simulating the response of cAMP and cPKA to a pulse of IBMX using the parameters in Table 1 in the main text except where noted in the captions. cAMP (panel (A)) rises rapidly to its new equilibrium in response to AC activity at the plasma membrane and diffuses rapidly throughout the cell, including the nucleus. Indeed, the spatial profile (panel (B)) is almost perfectly flat even during the upstroke. cPKA, on the other hand, though rapid to respond to the rise in cAMP at the plasma membrane and throughout the cytosol up to the nuclear membrane, rises slowly inside the nucleus owing to the assumed slow diffusion through the nuclear envelope (panel (C)) and the spatial profile during the upstroke is nearly a step function (panel (D)).

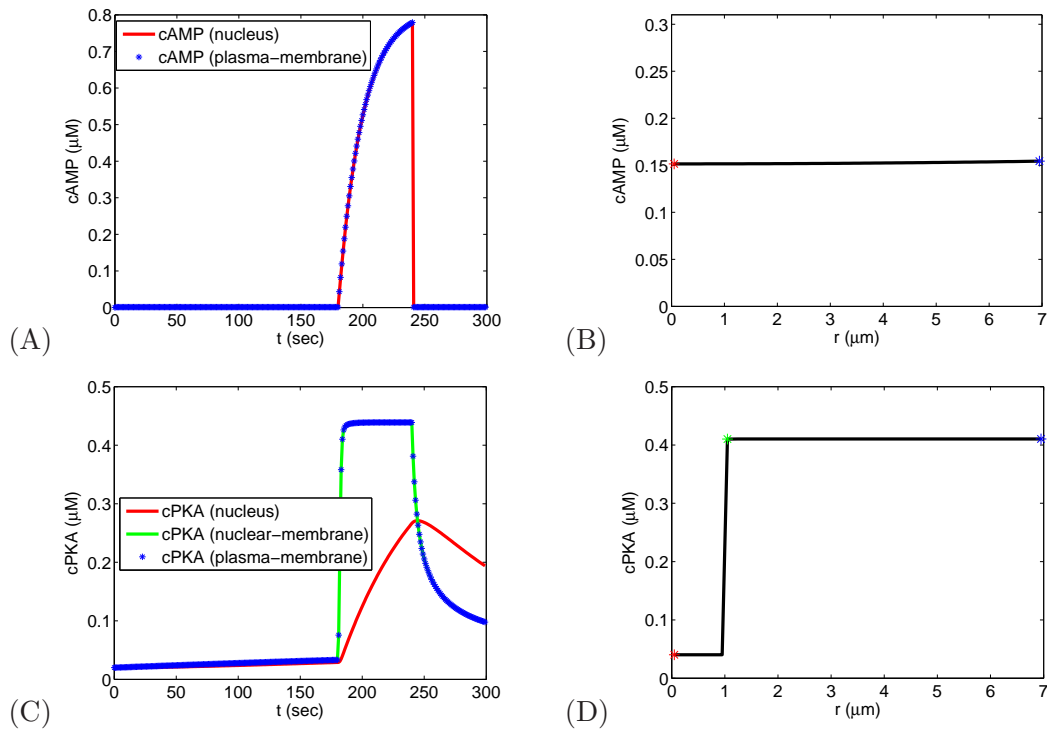


Figure S3: Rapid spatial equilibrium of cAMP and cPKA without labels. The spatial plots (B) and (D) are at $t = 180$ s. The colored spatial points in panels (B) and (D) indicate the corresponding curves for the time traces in (A) and (C). The parameters are as in Table 1 in the supplemental material except $g_a = 1.6454 \mu\text{M}/\text{s}$, $K_d = 0.0969 \mu\text{M}$, $C_T = 0.5 \mu\text{M}$, $R_{2T} = 0.2239 \mu\text{M}$, $R_{3T} = 0.5075 \mu\text{M}$, $k_{hi} = 1000/\text{s}$, and the effective diffusion across the nuclear membrane $D_N = 0.0005 \mu\text{m}^2\text{s}^{-1}$.

This confirms our fundamental hypothesis that hindered diffusion at the nuclear membrane is sufficient to account for the delayed rise in cPKA within the nucleus seen in experiments (?). Figure S3 also suggests that the full spatial partial differential equation description may not be required and that a three-compartment ODE model with sub-membrane, cytosolic, and nuclear compartments is sufficient (see Methods). We examine the range of validity of this approximation in the Figs. S4 and S5 (pp. S5, S6), where we also compare the effects of AC activation by forskolin and PDE inhibition

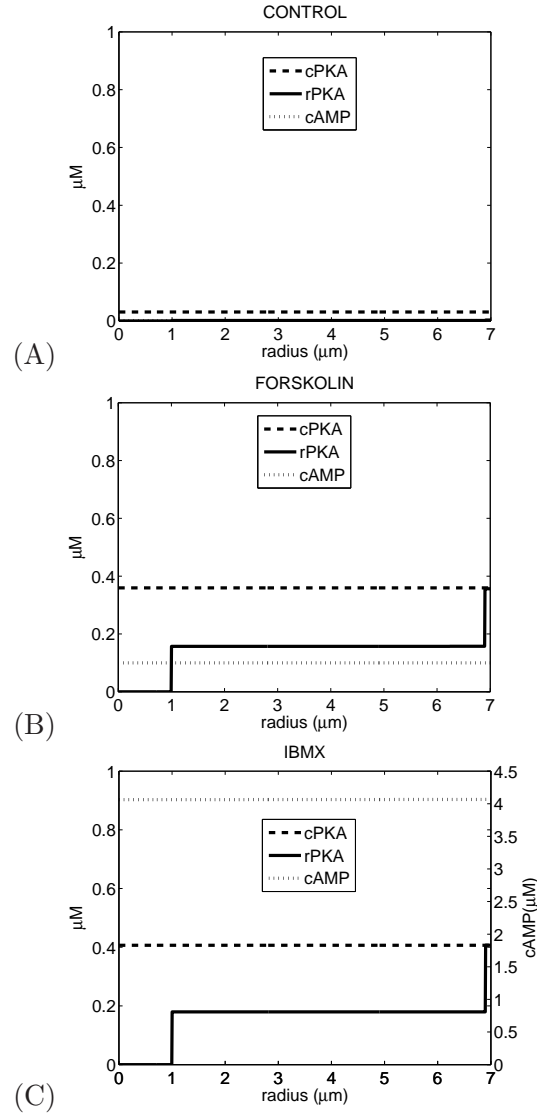


Figure S4: Steady-state PKA response to cAMP. (A) Control ($AC = 1\mu\text{M}/\text{s}$, $k_{pde_a} = 1000/\text{s}$, and $k_{pde_s} = 0.01/\text{s}$). (B) Forskolin ($AC = 100\mu\text{M}/\text{s}$ and $k_{pde_a} = 1000/\text{s}$ $k_{pde_s} = 0.01/\text{s}$). (C) IBMX ($AC = 1\mu\text{M}/\text{s}$, $k_{pde_a} = 0.01/\text{s}$, and $k_{pde_s} = 0.01/\text{s}$). (Note the separate y-axis for cAMP in (C).)

by IBMX.

Figure S4 shows the spatial distribution of cAMP, cPKA, and rPKA in basal (control) conditions, with low AC activity and with high PDE activity. In the basal condition (panel (A)), all three species are low and uniform across the cell. AC activation by forskolin (panel (B)) and PDE inhibition by IBMX (panel (C)) both result in an increase in cAMP throughout the cell, which leads to increases in free cPKA and rPKA in the cytosol as PKA holoenzyme is broken up. rPKA is excluded from the nucleus, but at steady state cPKA is spatially uniform across the nucleus and cytosol. The reduced level of rPKA in the cytosol is a result of the lower concentration of total rPKA (R_T) in the cytosol compared to the sub-membrane zone.

This figure also shows that IBMX and forskolin have similar effects in

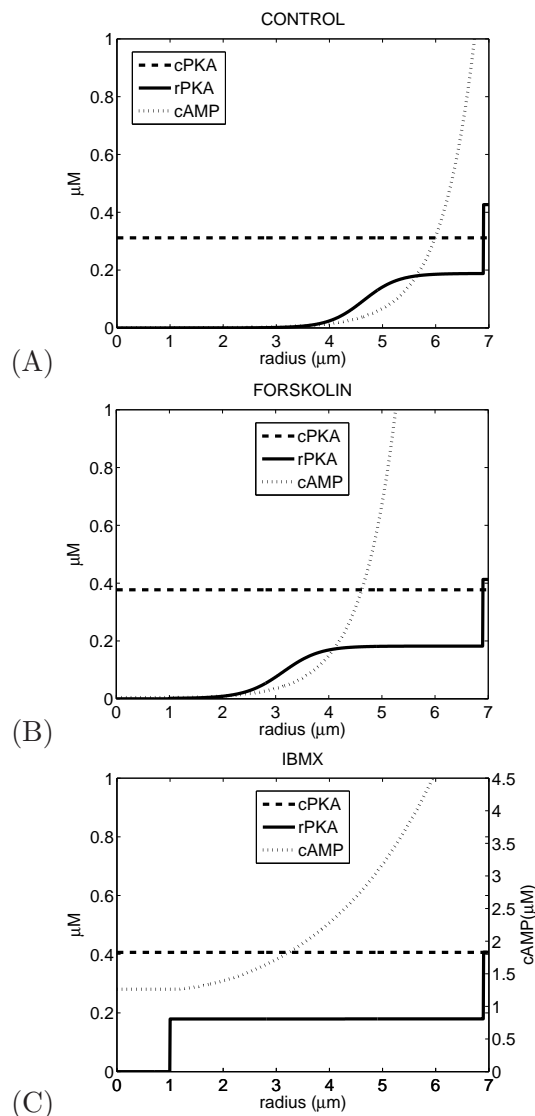


Figure S5: Steady-state PKA response to cAMP with higher flux of cAMP and higher activity of PDE to compensate. (A) Control ($AC = 3000\mu\text{M}/\text{s}$ and $k_{pde_a} = k_{pde_s} = 300/\text{s}$). (B) Forskolin ($AC = 30000\mu\text{M}/\text{s}$ and $k_{pde_a} = k_{pde_s} = 300/\text{s}$). (C) IBMX ($AC = 3000\mu\text{M}/\text{s}$ and $k_{pde_a} = k_{pde_s} = 30/\text{s}$). (Note the separate y -axis for cAMP in (C).)

the parameter regime suggested by the experiments, so the results of both the experiments and the modeling may be generalizable to AC activation and not just PDE inhibition. The cAMP in IBMX is larger than Forskolin due to the linearity assumptions of PDE activation. If saturation in PDE is taken into account, application of Forskolin can cause a more dramatic rise in cAMP. In Figure S4 downstream signaling would still be unaffected as maximal stimulation of cPKA is already achieved. However, in Figure S5 some gradient is maintained as a result.

For comparison, we show in Fig. S5 that spatial gradients in cAMP and rPKA persist even at steady state if the activity of AC is scaled up 3000-fold in the basal condition and 300-fold in the stimulated condition. If the

activity of PDE is also scaled up, this high flux can be made compatible with the data in (?).

With the higher level of AC activity, there is a gradient in cAMP and rPKA even in basal conditions, which is enhanced by both forskolin and IBMX. There is no gradient of cPKA at steady state because it is equalized by diffusion and the no-flux boundary conditions. Thus, the gradient in cPKA shown in Fig. S3(D) is only transient; if the stimulus were maintained indefinitely, the gradient would disappear. These considerations also show that a cAMP gradient cannot exclude cPKA from the nucleus on long timescales; we will consider later whether it could do so transiently.

rPKA equilibrates with cPKA based on the local concentration of cAMP and hence picks up the gradient from cAMP. The cAMP gradient in turn is dependent on degradation by PDE in the cytosol; if $k_{pde_s} = 0$, cAMP rapidly equilibrates uniformly to the boundary level of AC/k_{pde_a} . In Fig. S4, the gradient is very shallow because k_{pde_s} is small. Thus, unless a significant level of IBMX-resistant PDE is present, a cAMP gradient would not be expected in the conditions of (?).

These observations further support our hypothesis that the impediment to cPKA entry into the nucleus occurs at the nuclear envelope, and we proceed to investigate this further using the better-supported lower AC flux parameters, for which case a compartmental model, as described in the main text, suffices.

When Would a cAMP Gradient Be Present?

Rescaling the model shows that increased flux is equivalent to restricted cAMP diffusion or to making the cell larger. To see this, rewrite equations (S1)-(S3) in steady state as

$$\begin{aligned} 0 &= \frac{1}{r^2} \frac{\partial}{\partial r} \left(D_a(r) r^2 \frac{\partial a}{\partial r} \right) + f(a, C, r) \\ 0 &= \frac{1}{r^2} \frac{\partial}{\partial r} \left(D_c(r) r^2 \frac{\partial C}{\partial r} \right). \end{aligned}$$

Scaling the production and degradation of cAMP by α ($f \rightarrow \alpha f$) is equivalent to rescaling $D_a \rightarrow D_a/\alpha$ or rescaling space $r \rightarrow \sqrt{\alpha}r$. (Note that when rescaling space, the submembrane region must be rescaled as well.) For example, scaling the reaction rates by $\alpha = 3000$, the ratio of the rates in Fig. S5(C) to those in Fig. S4(C), would result in the same steady state as scaling D_a by a factor of 3000 to $0.033\mu\text{m}^2/\text{s}$ or scaling the β cell radius of $7\mu\text{m}$ by 54.8 ($\sqrt{3000}$) to $384\mu\text{m}$ with a submembrane compartment of $54.8 \cdot 100\text{nm} = 5.48\mu\text{m}$. Thus, either of these changes would also result in a gradient in cAMP, other things being equal.

We note that in larger cells, such as cardiac myocytes, there is direct experimental evidence that PDE plays an important role in confining cAMP to the sub-plasma membrane region (? ? ?), but the simulations here suggest that this is not important for the phenomena we are modeling in the β cell.

S4 Derivation of Equations for cAMP activation of PKA

From ?), we have the single compartment model of cAMP activation of PKA:



where PKA is $P = R : 2C$.

$k_{f1} = 13.0\mu M^{-2}s^{-1}$	$k_{b1} = 6.00 \times 10^{-3}s^{-1}$
$k_{f2} = 17.3\mu M^{-2}s^{-1}$	$k_{b2} = 6.00 \times 10^{-2}s^{-1}$
$k_{f3} = 5.10 \times 10^{-4}s^{-1}$	$k_{b3} = 4800\mu M^{-2}s^{-1}$

Table S1: Rate constants from (?) with the correction to the power on the units of concentration from the originally misstated nM^{-1} to nM^{-2} while leaving the value unchanged before converting to μM .

With the rPKA constraint of $R_T = R + C_1 + C_2 + P$, we have the system

$$\frac{dC_1}{dt} = -k_{f2}a^2C_1 + k_{b2}C_2 + k_{f1}a^2(R_T - C_1 - C_2 - R) - k_{b1}C_1 \quad (S7)$$

$$\frac{dC_2}{dt} = -k_{f3}C_2 + k_{b3}RC^2 + k_{f2}a^2C_1 - k_{b2}C_2 \quad (S8)$$

$$\frac{dC}{dt} = 2k_{f3}C_2 - 2k_{b3}RC^2 \quad (S9)$$

$$\frac{dR}{dt} = k_{f3}C_2 - k_{b3}RC^2 \quad (S10)$$

If we assume quasi-steady state for the complexes C_1 and C_2 , we get the reduction

$$\frac{dC}{dt} = 2q(a)(R_T - R) - 2(k_{b3} - k_{f3}w(a))RC^2 \quad (S11)$$

$$\frac{dR}{dt} = q(a)(R_T - R) - (k_{b3} - k_{f3}w(a))RC^2 \quad (S12)$$

where

$$q(a) = \frac{k_{f2}a^2\alpha}{\gamma(k_{f3} + k_{b2}) + k_{f2}a^2\beta}$$

$$w(a) = \frac{\gamma k_{b3}}{\gamma(k_{f3} + k_{b2}) + k_{f2}a^2\beta}$$

and $\alpha = k_{f1}a^2$, $\beta = k_{f1}a^2 - k_{b2}$ and $\gamma = a^2(k_{f1} + k_{f2}) + k_{b1}$. Note that this approximation (S11), (S12) to (S7)-(S10) has an excessive decay rate. If k_{b2}

is a factor of 10 larger (k_{b1} ineffective) then the approximation is excellent. We further simplify equations (S11) and (S12) with the approximation

$$\frac{dC}{dt} = 2k_b(a)(R_T - R) - 2k_a RC^2 \quad (\text{S13})$$

$$\frac{dR}{dt} = k_b(a)(R_T - R) - k_a RC^2 \quad (\text{S14})$$

where $k_b(a) = g_a a^2 / (a^2 + K_d^2)$, and we fit g_a , k_a , and K_d to the Dyachok data. (See Section S7)

S5 Compartmental Models with Labeled Species

In this section are the full models from which we create Figures 3, 4, and 6 in the main text.

Epifluorescence Model

Nucleus

$$\begin{aligned} C'_1 &= S_1/V_1 D_1/rh_1 (C_2 - C_1) \\ Z'_1 &= S_1/V_1 D_1/rh_1 (Z_2 - Z_1) \end{aligned}$$

Cytosol

$$\begin{aligned} R'_2 &= -k_a(C_2^2 + 2C_2 Z_2 + Z_2^2)R_2 + k_b(a_2)(P_{r2c2} + 2P_{rcz2} + P_{r2z2}) \\ P'_{r2c2} &= k_a C_2^2 R_2 - k_b(a_2)(P_{r2c2}) \\ P'_{r2z2} &= k_a Z_2^2 R_2 - k_b(a_2)(P_{r2z2}) \end{aligned}$$

Boundary

$$\begin{aligned} C'_3 &= -S_2/V_3 D_2/rh_2 (C_3 - C_2) - 2k_a(C_3^2 + C_3 Z_3)R_3 + 2k_b(a_3)(P_{r2c3} + P_{rcz3}) \\ Z'_3 &= -S_2/V_3 D_2/rh_2 (Z_3 - Z_2) - 2k_a(Z_3^2 + C_3 Z_3)R_3 + 2k_b(a_3)(P_{r2z3} + P_{rcz3}) \\ R'_3 &= -k_a(C_3^2 + 2C_3 Z_3 + Z_3^2)R_3 + k_b(a_3)(P_{r2c3} + 2P_{rcz3} + P_{r2z3}) \\ P'_{r2c3} &= k_a C_3^2 R_3 - k_b(a_3)(P_{r2c3}) \\ P'_{r2z3} &= k_a Z_3^2 R_3 - k_b(a_3)(P_{r2z3}) \end{aligned}$$

cAMP

$$\begin{aligned} a'_1 &= -k_{pdes} a_1 + S_1/V_1 D a_1 (a_2 - a_1)/rh_1 \\ a'_2 &= -k_{pdes} a_2 + S_2/V_2 D a_2 (a_3 - a_2)/rh_2 - S_1/V_2 D a_1 (a_2 - a_1)/rh_1 \\ a'_3 &= AC - k_{pde_a} a_3 - k_{pde_s} a_3 - S_2/V_3 D a_2 (a_3 - a_2)/rh_2 \end{aligned}$$

Constraints

$$\begin{aligned} R_{2T} &= (V R_T - V_3 R_{3T})/V_2 \\ Z_2 &= (V Z_T - V_1 Z_1 - V_3 Z_3 - V_2 P_{r2z2} - V_3 P_{r2z3} - V R_T + R_2 V_2 + V_2 P_{r2c2} + V_3 R_3 + V_3 P_{r2c3})/V_2 \\ C_2 &= (V C_T - V_1 C_1 - V_3 C_3 - V_2 P_{r2c2} - V_3 P_{r2c3} - V R_T + R_2 V_2 + V_2 P_{r2z2} + V_3 R_3 + V_3 P_{r2z3})/V_2 \\ P_{rcz2} &= (1/2)(V R_T - V_3 R_{3T} - R_2 V_2 - V_2 P_{r2c2} - V_2 P_{r2z2})/V_2 \\ P_{rcz3} &= (1/2)R_{3T} - (1/2)R_3 - (1/2)P_{r2c3} - (1/2)P_{r2z3} \end{aligned}$$

TIRF Model

Constraints

$$\begin{aligned}
R_{2T} &= (VR_T - V_3R_{3T})/V_2 \\
X_{2T} &= (VX_T - V_3X_{3T})/V_2 \\
C_2 &= (VC_T - V_1C_1 - V_3C_3 - 2V_2(R_{2T} - R_2) - 2V_3(R_{3T} - R_3) - V_2P_{xc2} - V_3P_{xc3})/V_2 \\
Y_2 &= (VY_T - V_3Y_3 - V_2(X_{2T} - X_2) - V_3(X_{3T} - X_3) + V_3P_{xc3})/V_2
\end{aligned}$$

Nucleus

$$C'_1 = S_1/V_1D_1/rh_1(C_2 - C_1)$$

Cytosol

$$\begin{aligned}
R'_2 &= -k_aC_2^2R_2 + k_b(a_2)(R_{2T} - R_2) \\
X'_2 &= -k_aY_2X_2 + k_b(a_2)(X_{2T} - X_2 - P_{xc2}) - k_aC_2X_2 + k_b(a_2)P_{xc2} \\
P'_{xc2} &= k_aC_2X_2 - k_b(a_2)P_{xc2}
\end{aligned}$$

Boundary

$$\begin{aligned}
C'_3 &= -S_2/V_3D_2/rh_2(C_3 - C_2) - 2k_aC_3^2R_3 + 2k_b(a_3)(R_{3T} - R_3) - k_aC_3X_3 + k_b(a_3)P_{xc3} \\
R'_3 &= -k_aC_3^2R_3 + k_b(a_3)(R_{3T} - R_3) \\
Y'_3 &= -S_2/V_3D_2/rh_2(Y_3 - Y_2) - k_aY_3X_3 + k_b(a_3)(X_{3T} - X_3 - P_{xc3}) \\
X'_3 &= -k_aY_3X_3 + k_b(a_3)(X_{3T} - X_3 - P_{xc3}) - k_aC_3X_3 + k_b(a_3)P_{xc3} \\
P'_{xc3} &= k_aC_3X_3 - k_b(a_3)P_{xc3}
\end{aligned}$$

cAMP

$$\begin{aligned}
a'_1 &= -k_{pde_s}a_1 + S_1/V_1Da_1(a_2 - a_1)/rh_1 \\
a'_2 &= -k_{pde_s}a_2 + S_2/V_2Da_2(a_3 - a_2)/rh_2 - S_1/V_2Da_1(a_2 - a_1)/rh_1 \\
a'_3 &= AC - k_{pde_a}a_3 - k_{pde_s}a_3 - S_2/V_3Da_2(a_3 - a_2)/rh_2
\end{aligned}$$

S6 Details of Time Scale Analysis

In this section we carry out the details of the time-scale analysis whose results are discussed in the main text (see Eq. 12 and following text). The analysis shows explicitly that the nuclear cPKA is the slowest variable and how it depends on the frequency of the IBMX stimulus. There are three time scales inherent in this system. 1) Fast: Diffusion of cAMP and cPKA $\approx 100 \mu\text{m}^2/\text{s}$. Scaling this by the cell radius $7\mu\text{m}$ yields a reciprocal time constant of $\approx 2\text{s}$. The cAMP dependent binding and unbinding of cPKA from rPKA is also of the same order; 2) Intermediate: The period of IBMX stimulation is chosen to correspond to the period of calcium bursting at about 4 min yielding a frequency of $0.25/\text{min} \approx 0.004/\text{s}$; 3) Slow: The diffusion through the nuclear pore has a time constant of about 30 min (?), which translates into a nuclear diffusion coefficient D_N . If we let $\delta = S_1D_N/(V_1rh_1)$ be about $1/30\text{min}$, then $D_N \approx 6e^{-4}\mu\text{m}^2/\text{s}$.

Forcing by IBMX generates quasi-steady state cAMP (a) leading to

$$R_2 = \frac{R_{2T}k_d(a_2)}{C_2^2 + k_d(a_2)}, \quad R_3 = \frac{R_{3T}k_d(a_3)}{C_3^2 + k_d(a_3)}.$$

Outside of the nucleus, cPKA would rapidly equilibrate to a periodic quasi-steady state as well, which can be described by a periodic function χ

$$C_2 = C_3 = C_{23}^* \equiv \chi(\omega t) \approx C^*.$$

Nuclear cPKA, C_1 , would follow the periodic forcing by cytosolic cPKA more or less faithfully depending on its own time constant. Letting $\tau = \omega t$, we are left with the single equation for C_1

$$\frac{dC_1}{d\tau} = -\varepsilon(C_1 - \chi(\tau)) \quad (\text{S15})$$

where $\varepsilon = \delta/\omega$. Dividing the value of δ estimated above by $\omega = 1/4\text{min}$ gives $\varepsilon \approx 2/15$. The non-dimensional parameter ε must be small to account for the behavior described in Fig. 3, i.e. δ must be small compared to ω , which is set by the experimental protocol. The only plausible source of the slow time scale in the problem then is D_N , the diffusion rate across the nuclear membrane.

The linear non-autonomous ODE (S15) can be solved in terms of $\chi(\tau)$, but exploiting the time scales is illustrative. Treating the problem as a regular perturbation problem produces undesirable secular terms that grow like $\varepsilon\tau$, so we treat the two slowest time scales as independent variables, $\tau_1 = \tau$ and $\tau_2 = \varepsilon\tau$, having already used the fastest time scale to equilibrate extranuclear cPKA to $\chi(\tau_1)$. We get

$$\frac{dC_1(\tau_1, \tau_2)}{d\tau} = \frac{\partial C_1(\tau_1, \tau_2)}{\partial \tau_1} + \varepsilon \frac{\partial C_1(\tau_1, \tau_2)}{\partial \tau_2} = -\varepsilon(C_1(\tau_1, \tau_2) - \chi(\tau_1)). \quad (\text{S16})$$

Now we assume an expansion in ε , $C_1(\tau_1, \tau_2) = y_0(\tau_1, \tau_2) + \varepsilon y_1(\tau_1, \tau_2) + \varepsilon^2 y_2(\tau_1, \tau_2) + \dots$, and we see that to zeroth order in ε

$$\frac{\partial y_0(\tau_1, \tau_2)}{\partial \tau_1} = 0,$$

so $y_0(\tau_1, \tau_2) = y_0(\tau_2)$. The next order equation

$$\frac{\partial y_1(\tau_1, \tau_2)}{\partial \tau_1} = -\frac{dy_0(\tau_2)}{d\tau_2} - y_0(\tau_2) + \chi(\tau_1) \quad (\text{S17})$$

requires the solution of the solvability condition which has the integral over the period of the forcing function

$$0 = \int_0^T \left[-\frac{dy_0(\tau_2)}{d\tau_2} - y_0(\tau_2) + \chi(s) \right] ds,$$

yielding the slow time scale equation

$$0 = -\frac{dy_0(\tau_2)}{d\tau_2} - y_0(\tau_2) + \frac{1}{T} \int_0^T \chi(s) ds \quad (\text{S18})$$

with solution

$$y_0(\tau_2) = A(1 - e^{-\tau_2}) \quad (\text{S19})$$

where $A = \frac{1}{T} \int_0^T \chi(s) ds$ is the average of χ over a period, assuming that the initial nuclear cPKA concentration is 0. The $O(\varepsilon)$ equation (S17) becomes

$$\frac{\partial y_1(\tau_1, \tau_2)}{\partial \tau_1} = \chi(\tau_1) - A$$

with solution

$$y_1(\tau_1, \tau_2) = \int_0^{\tau_1} [\chi(s) - A] ds + f(\tau_2),$$

where $f(\tau_2)$ is the constant of integration with respect to τ_1 . To find $f(\tau_2)$ we look to the $O(\varepsilon^2)$ equation

$$\frac{\partial y_2(\tau_1, \tau_2)}{\partial \tau_2} = -\frac{\partial y_1(\tau_1, \tau_2)}{\partial \tau_1} - y_1(\tau_1, \tau_2)$$

and the solvability condition

$$0 = -\frac{df(\tau_2)}{d\tau_2} - f(\tau_2) + \frac{1}{T} \int_0^T \int_0^s [\chi(\xi) - A] d\xi.$$

However, the last term in the equation is an integral over the period of a function with zero average, so in conjunction with the zero initial condition, $f(\tau_2) = 0$, and $y_1(\tau_1, \tau_2) = y_1(\tau_1) = \int_0^{\tau_1} [\chi(s) - A] ds$. Thus, through first order

$$C_1(\tau_1, \tau_2) = A(1 - e^{-\tau_2}) + \varepsilon \int_0^{\tau_1} [\chi(s) - A] ds + O(\varepsilon^2),$$

or in terms of t

$$C_1(t) = A(1 - e^{-\delta t}) + \frac{\delta}{\omega} \int_0^{\omega t} [\chi(s) - A] ds + O(\varepsilon^2)$$

or

$$C_1(t) = A(1 - e^{-\delta t}) + \delta \int_0^t [\chi(\omega s) - A] ds + O(\varepsilon^2).$$

$\chi(t)$ is fast and hence rapidly equilibrates with the stimulus IBMX (Eq. 1 in the supplemental material), which is a square wave. Thus, we get

$$\chi(t) = \begin{cases} C_{lo}, & (N-1)T < t < \rho NT \\ C_{hi}, & \rho NT < t < NT \end{cases}$$

for $N = \{1, 2, 3, \dots\}$ and $0 < \rho < 1$, we get

$$A = (1 - \rho)C_{hi} + \rho C_{lo} \quad (\text{S20})$$

where T is the period of IBMX stimulation. For the experiments in (?), $T = 240\text{s}$ and $\rho T = 180\text{s}$ so that $A = \frac{1}{4}C_{hi} + \frac{3}{4}C_{lo}$.

This approximation captures the early transients and long time average behavior but the potential variation that exists on top of the average behavior at long times is not captured with a finite number of higher order terms. However, the apparent separation between the average behavior on the slower time scale in the first order term of the multiscale approximation and the oscillatory higher order behavior on the faster time scale encourages us to decompose $C_1(t)$ without expansion.

Long-time, higher-order behavior dependence on period

In order to understand better the dependence of the cPKA oscillation on the period of the stimulus, we break down the solution C_1 as

$$C_1(t) = y_0(\tau_2) + x(\tau_1). \quad (\text{S21})$$

For changes that force x to be small, C_1 tracks the y_0 behavior. Plugging this decomposition of C_1 into (S15) and using equation (S18) yields the following equation for x

$$\frac{dx}{d\tau_1} = -\varepsilon(x - (\chi(\tau_1) - A))$$

with solution

$$x(\tau_1) = \varepsilon e^{-\varepsilon\tau_1} \int_0^{\tau_1} e^{\varepsilon s} (\chi(s) - A) ds.$$

There is a slow time scale dependence whose first term in an expansion in ε produces the second term in the multiscale approximation. We show the behavior of C_1 as the average behavior plus an amplitude of deviation in Fig. 5 in the main text.

S7 Parameter Fitting

We fit the three-compartment model to match the TIRF and EPI data of ?) obtained with IBMX pulses. We construct an objective function as the difference between model and measured fluorescence values. The vector of fluorescence measures at steady state is

$$f = [Epi_{IBMXoff}, Epi_{IBMXon}, TIRF_{IBMXoff}, TIRF_{IBMXon}].$$

The epifluorescence experiment and the TIRF experiment each with and without IBMX applied are used and the effect of IBMX is assumed to be a decrease in k_{pde_a} . The measured values are $f^\# = [0.6, 0.95, 1.0, 1.8]$. We minimize the squared L^2 norm of their difference, $\|f - f^\#\|^2$, over the parameters R_{3T}, R_{2T}, g_a , and K_d . We also allow variation in C_T , and Z_T in the epi experiments and C_T, Y_T, X_T , and X_{3T} in the TIRF experiments, while fixing γ , and ε . Parameters allowed to vary are shown with an (*) in Table S3.

Parameter Sensitivity

In this section we look at two ways of understanding the model's sensitivity to parameters. First we perform a systematic perturbation of the model parameters and show the effect on the measures used for fitting the parameters (called the "misfit"). We then analyze aspects of these sensitive parameters that are independent.

In Table S2 (p. S15) we show the effects on the fitting measure defined above, $\|f - f^\#\|^2$, of 2, 5 and 10 fold factor increases in each parameter independently. In Table S3 (p. S16) we show the effects of a $\pm 10\%$ independent perturbation of each parameter, along with the specific changes in the Epi and TIRF values; the latter are omitted in Table S2 for brevity, but an idea of the magnitudes can be obtained by comparing the misfits.

The effects of the parameters that have the greatest sensitivity are

- (XTT) total labeled rPKA in the TIRF study: Increase or decrease shifts both the hi and lo TIRF ratio down or up, respectively.
- (X3T) submembrane labeled rPKA in the TIRF study: Increase or decrease shifts primarily the hi TIRF ratio down or up, respectively.
- (YT) total labeled cPKA in the TIRF study: Increase or decrease shifts both the hi and lo TIRF ratio up or down, respectively.
- (ZT) total labeled cPKA in the Epi study: Decrease leads to drop in Epi ratio and amount of cPKA that can enter the nucleus in the basal state.
- (AC) Adenylyl cyclase: Increasing or decreasing AC leads to an increase or decrease in both of the basal Epi and TIRF ratios and thus, the amount of cPKA that can enter the nucleus in the basal state.
- (ga) Dissociation rate of cPKA: Increasing or decreasing this rate primarily effects the TIRF ratio in high cAMP by increasing or decreasing, respectively.
- (Kd) cPKA dissociation constant: Decreasing affinity of cAMP for PKA (increasing Kd) leads to a slight increase in both basal Epi and TIRF ratios as the basal cAMP becomes more effective.
- (khi) Basal IBMX-sensitive PDE activity: Decreasing k_{hi} leads to an increase in Epi and TIRF ratios due to slightly higher basal cAMP.

Some parameters are not completely independent. For example, if AC and khi are both reduced by the same factor then cAMP production attains the same steady level but less rapidly. Note that as long as cAMP rises rapidly enough to sufficiently high levels (i.e. near the PKA dissociation constant, K_d), the cPKA dynamics change little because cAMP production is still much faster than cPKA liberation. Similarly, if AC is altered but is compensated by a change in the PKA sensitivity to the cAMP levels (i.e. K_d), then cPKA dynamics are effectively unaltered. If we alter the levels of both labeled rPKA and labeled cPKA in the TIRF experiments, the change is significantly less dramatic than if we change each individually.

Var	Misfit ($\times 2$)	Misfit ($\times 5$)	Misfit ($\times 10$)
Baseline	2.30e-05	2.30e-05	2.30e-05
Da	2.32e-05	2.33e-05	2.34e-05
DN	2.30e-05	2.30e-05	2.30e-05
ReTT*	2.51e-03	1.51e-02	3.33e-02
Re3T*	1.58e-04	1.70e-03	7.92e-03
RtTT*	5.82e-05	2.06e-04	3.82e-04
Rt3T*	2.30e-05	2.30e-05	2.30e-05
CeT*	7.12e-05	4.87e-04	1.67e-03
CtT*	1.11e-03	1.36e-02	5.86e-02
XTT*	6.04e-01	1.22e+01	6.54e+01
X3T*	6.84e-01	3.30e+00	5.39e+00
YT*	8.61e-01	2.37e+00	3.16e+00
ZT*	1.74e-03	1.10e-02	2.38e-02
AC	1.07e-02	1.21e-01	3.53e-01
kpde	2.30e-05	2.30e-05	2.30e-05
kpde2	3.38e-05	2.75e-04	2.06e-03
ga*	3.80e-02	1.58e-01	2.59e-01
Kd*	3.40e-03	2.90e-02	1.42e-01
khi	2.88e-03	8.03e-03	1.06e-02
klow	3.23e-04	1.20e-02	8.72e-02

Table S2: Parameter Sensitivity Study. We increase the parameters from Table 1 in the main text and listed under (Var) by factors of 2, 5, and 10. The * refers to parameters that were fit. “Misfit” refers to the magnitude of the fitting measure $\|f - f^\#\|^2$ defined in the text and should be compared to “Baseline”.

Var	Misfit	Epi _{lo}	Epi _{hi}	TIRF _{lo}	TIRF _{hi}
Baseline	2.30e-05	0.60	0.95	1.00	1.80
Da-	2.30e-05	0.60	0.95	1.00	1.80
Da+	2.31e-05	0.60	0.95	1.00	1.80
DN-	2.30e-05	0.60	0.95	1.00	1.80
DN+	2.30e-05	0.60	0.95	1.00	1.80
ReTT*-	6.60e-05	0.61	0.95	1.00	1.80
ReTT*+	7.65e-05	0.60	0.94	1.00	1.80
Re3T*-	2.01e-05	0.60	0.95	1.00	1.80
Re3T*+	2.79e-05	0.60	0.95	1.00	1.80
RtTT*-	2.25e-05	0.60	0.95	1.00	1.80
RtTT*+	2.44e-05	0.60	0.95	1.00	1.80
Rt3T*-	2.30e-05	0.60	0.95	1.00	1.80
Rt3T*+	2.30e-05	0.60	0.95	1.00	1.80
CeT*-	2.16e-05	0.60	0.95	1.00	1.80
CeT*+	2.51e-05	0.60	0.95	1.00	1.80
CtT*-	3.99e-05	0.60	0.95	1.00	1.80
CtT*+	3.28e-05	0.60	0.95	1.00	1.80
XTT*-	2.69e-03	0.60	0.95	0.96	1.77
XTT*+	3.16e-03	0.60	0.95	1.05	1.83
X3T*-	1.39e-02	0.60	0.95	0.99	1.68
X3T*+	1.21e-02	0.60	0.95	1.01	1.91
YT*-	4.25e-02	0.60	0.95	1.07	1.99
YT*+	2.80e-02	0.60	0.95	0.94	1.64
ZT*-	3.96e-05	0.61	0.95	1.00	1.80
ZT*+	6.23e-05	0.60	0.94	1.00	1.80
AC-	1.13e-04	0.59	0.95	0.99	1.80
AC+	1.66e-04	0.61	0.95	1.01	1.80
kpde-	2.30e-05	0.60	0.95	1.00	1.80
kpde+	2.30e-05	0.60	0.95	1.00	1.80
kpde2-	2.31e-05	0.60	0.95	1.00	1.80
kpde2+	2.31e-05	0.60	0.95	1.00	1.80
ga*-	1.00e-03	0.60	0.94	1.00	1.77
ga*+	8.15e-04	0.61	0.95	1.00	1.83
Kd*-	1.96e-04	0.61	0.95	1.01	1.80
Kd*+	9.45e-05	0.60	0.95	0.99	1.80
khi-	1.93e-04	0.61	0.95	1.01	1.80
khi+	9.07e-05	0.60	0.95	0.99	1.80
klow-	2.39e-05	0.60	0.95	1.00	1.80
klow+	2.53e-05	0.60	0.95	1.00	1.80

Table S3: Parameter Sensitivity Study on Fine Scale. We perturb the parameters from Table 1 in the main text and listed under (Var) down (-) or up(+) by 10%. The * refers to parameters that were fit. “Misfit” is as in Table S2. Each of the other columns is an element of the fitting measure vector to show where the measure changes. (Note: For the subscripts on Epi and TIRF, *lo* = *IBMXoff* and *hi* = *IBMXon* for comparison with the fitting measure.)